Supporting Information

Bifunctional polypyrrole-based conductive paper towards simultaneously efficient solar-driven water evaporation and electrochemical energy storage

Jiahong Zhang[1#], Pengfei Wang[2#], Yulian Chen[1], Xiaojiang Mu[1], Xiaoyang Wang[1,2], Sakae Tanemura[3], Jianhua Zhou[1]*, Lei Miao[1]*

[1]Guangxi Key Laboratory of Information Materials, Engineering Research Center of Electronic Information Materials and Devices，Ministry of Education, School of Material Science and Engineering, Guilin University of Electronic Technology, Guilin 541004, China

[2]Department of Chemical Systems Engineering, Graduate School of Engineering, Nagoya University, Nagoya, 4648603, Japan

[3]Japan Fine Ceramic Center 2-4-1 Mutsuno, Atsuta-ku, Nagoya 456-8587, Japan

# These authors contributed equally to this work.

*Corresponding Author

E-mail: jianhuazhou@guet.edu.cn; lead contact: miaolei@guet.edu.cn

Material Characterizations

The surface morphology and microstructure of the samples were observed by scanning electron microscopy (SEMS-4800, Hitachi, Japan). The samples were characterized by Fourier transform infrared (FTIR, Bruker, TENSOR27, U.S.A.) spectra. The characteristic peaks were measured by a Raman scattering measuring device (HORIBA, Lab RAM HR Evolution, France). The absorption spectrum over 250-2500 nm of the samples were recorded via a UV-Vis-NIR spectrometer (JASCO V-570, Japan). The detailed scans for C 1s and N 1s were measured by X-ray photoelectron spectra (Thermo Fisher, ESCALAB250Xi, USA). The water contact angles (WCAs) of different kinds of samples were measured using a contact angle analyzer (JC2000D1, Powereach Co., China). Real-time mass loss monitoring was achieved by an electronic balance (ATX224, Shimadzu, Japan). The electrochemical properties were measured by using an electrochemical workstation (Vretex.One.EIS, Ivium, Holland).

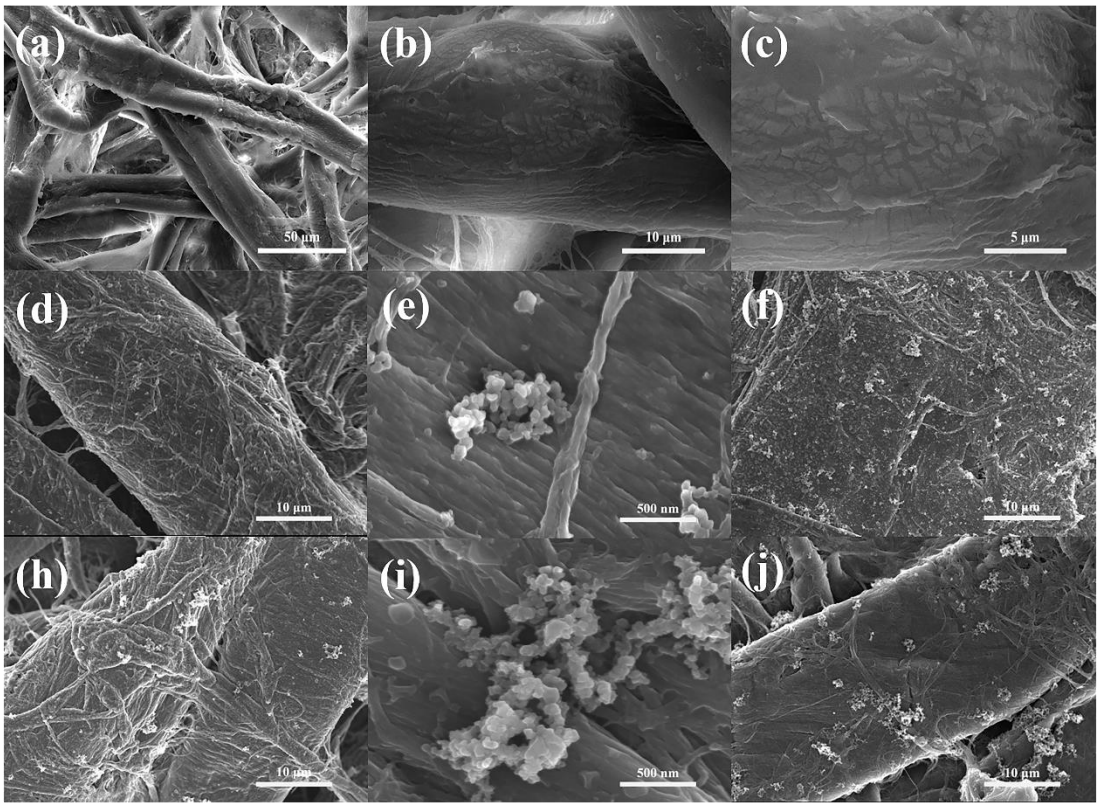

Figure S1. The SEM images for (a-c) the blank filter paper at different magnifications, (c-d) PPy-100 filter paper at different magnifications, (f) PPy-150 filter paper, (h-i) PPy-250 filter paper at different magnifications, (j) PPy-300 filter paper.

Table S1. The loading mass of PPy/filter paper with different dosages.

Samples	The loading mass (mg cm^{-2})
PPy-100	2.93
PPy-150	3.83
PPy-200	4.24
PPy-250	4.77
PPy-300	5.58

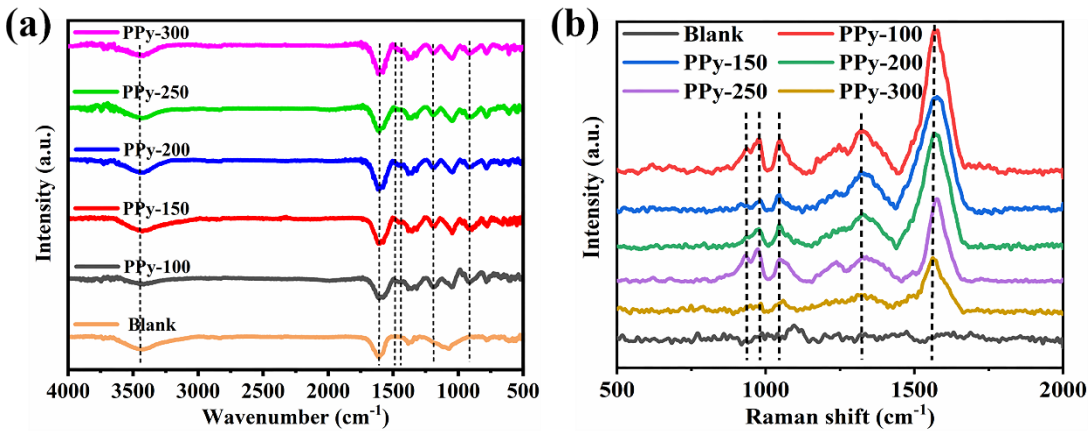

Figure S2. (a) FTIR spectra and (b) Raman spectra for the blank filter paper, PPy-100, 150, 200, 250, 300 filter paper.

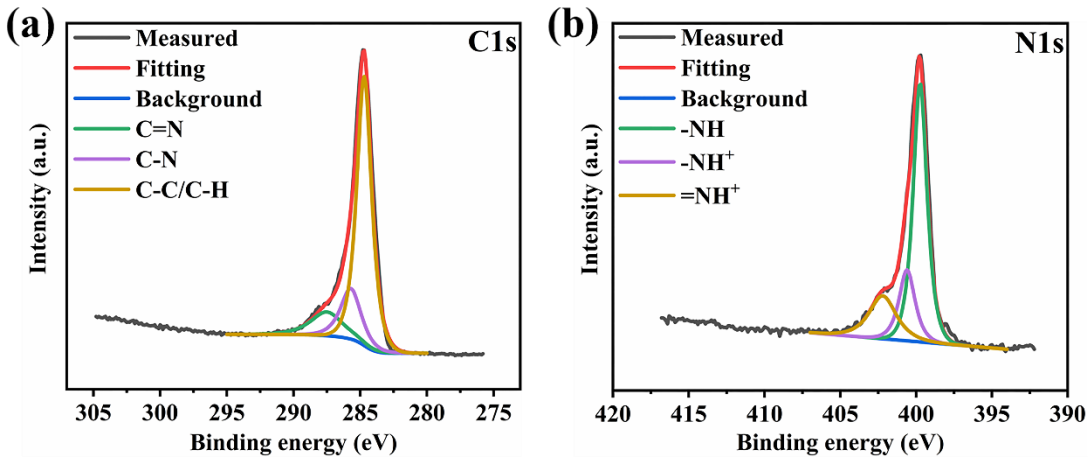

Figure S3. The XPS survey spectra for (a) C 1s, (b) N 1s of the PPy-200 filter paper.

Figure S4. The digital photos of the PPy/filter paper soaked in water for 7 days.

Table S2. Comparison of performance of flexible PPy-based materials.

Materials	Capacitance (mF cm^{-2})	Reference
PPy/RGO/bacterial cellulose paper	2100 mF cm^{-2} at 2 mA cm^{-2}	[1]
Ni-CAT-MOF/PPy foam	1050 mF cm^{-2} at 0.5 mA cm^{-2}	[2]
PPy/MoS_2/Carbon cloth	1150.4 mF cm^{-2} at 1 mA cm^{-2}	[3]
PPy/Air-Laid paper	3100 mF cm^{-2} at 1 mA cm^{-2}	[4]
ECNT/PPy	965.3 mF cm^{-2} at 1 mA cm^{-2}	[5]
Ni_3S_2@PPy/NF	3148.0 mF cm^{-2} at 2 mA cm^{-2}	[6]
MoS_2-DBS-PPy film	1200 mF cm^{-2} at 0.5 mA cm^{-2}	[7]

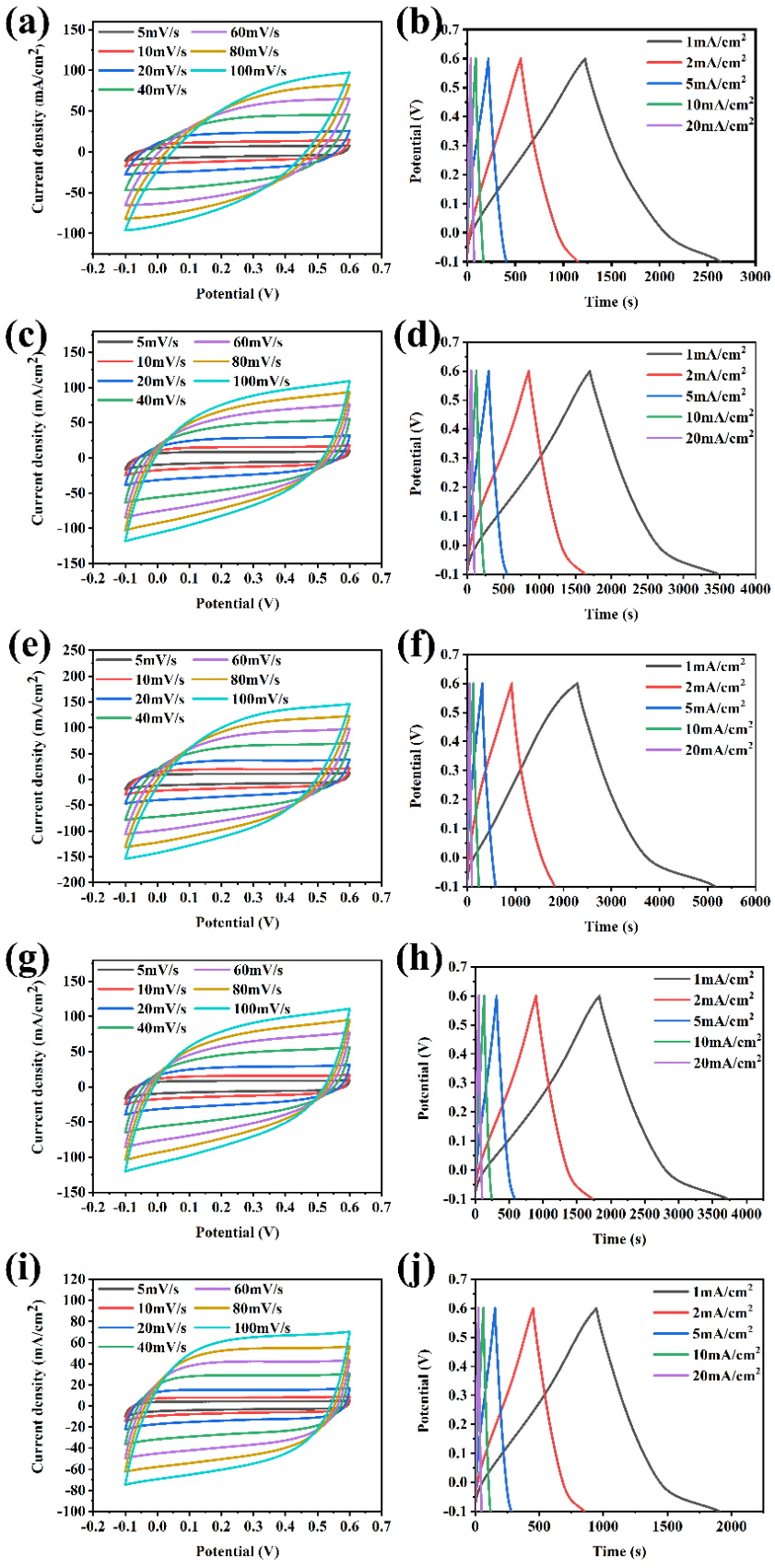

Figure S5. CV cures at different scan rates and GCD curves at different current densities for PPy-100 (a-b), 150 (c-d), 200 (e-f), 250 (g-h), 300 (i-j) filter paper, respectively.

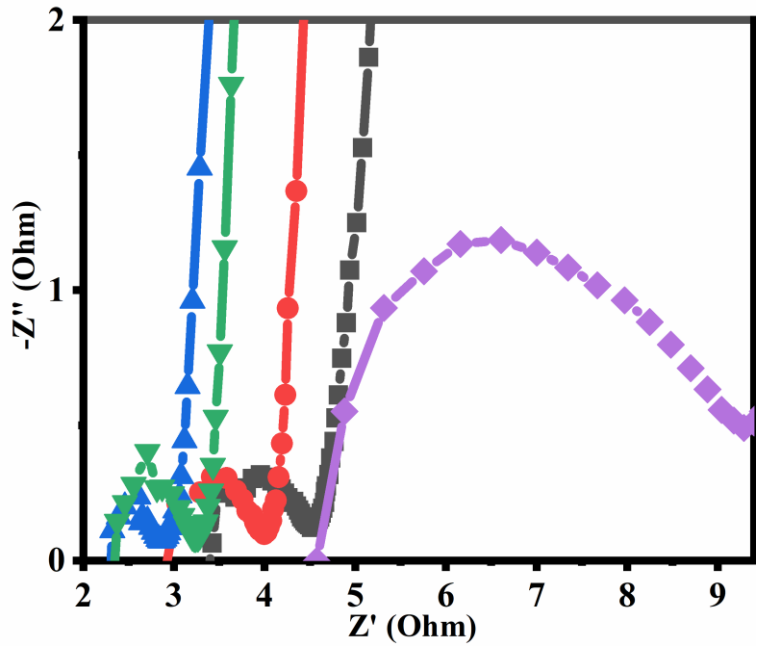

Figure S6. The local magnification image of the EIS curve for the PPy-100, 150, 200, 250, 300 filter paper electrode in the high-frequency band.

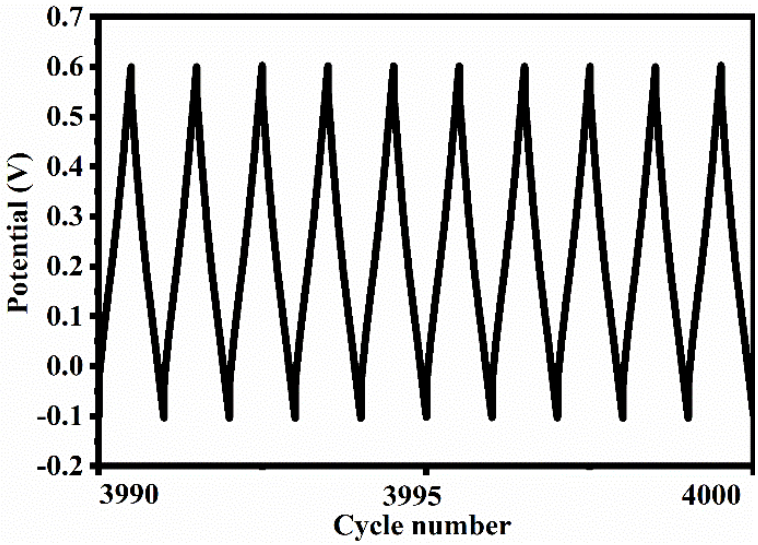

Figure S7. The GCD curve of the PPy-200 filter paper electrode from the 3990th to the 4000th cycle.

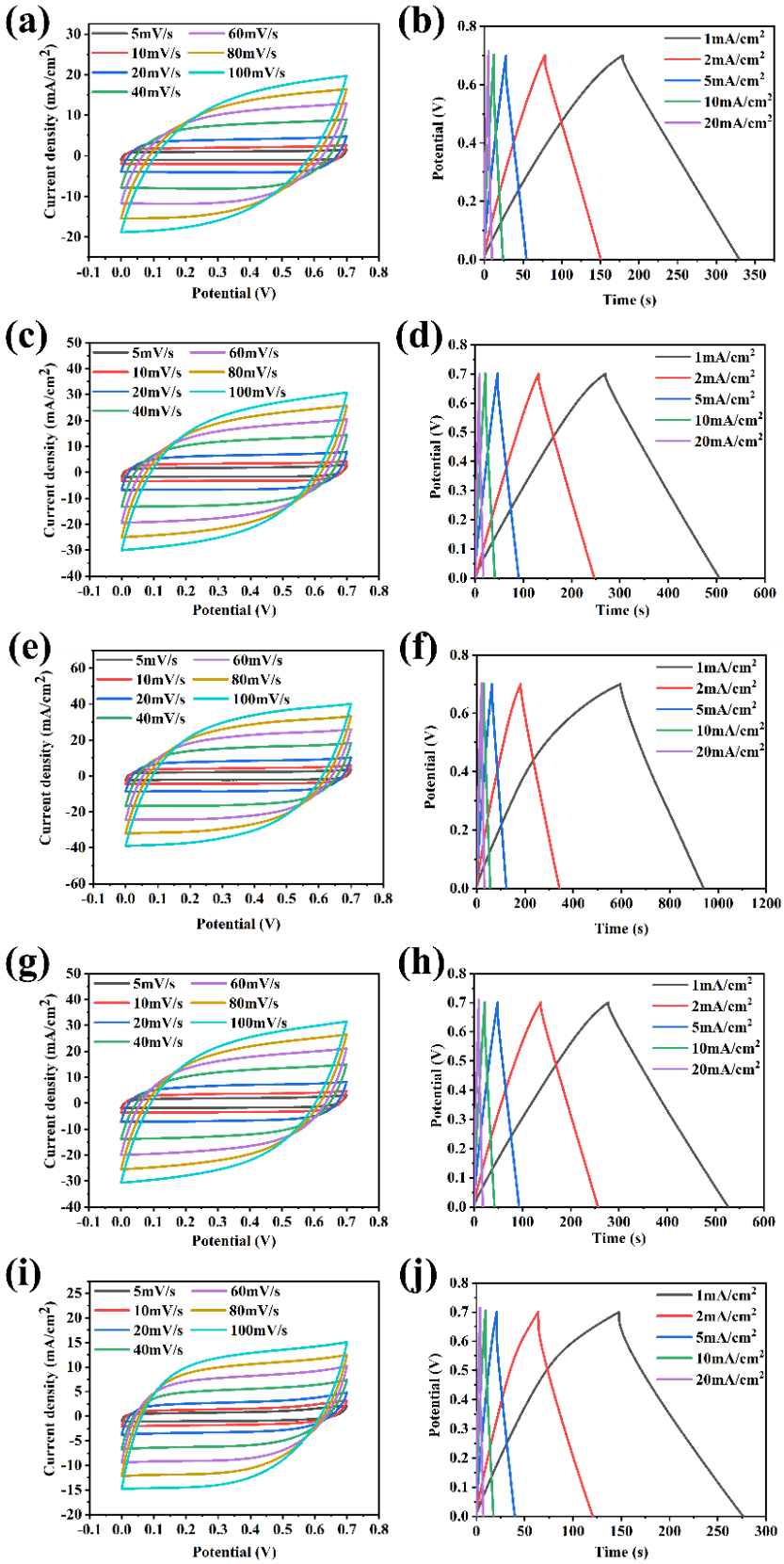

Figure S8. CV cures at different scan rates and GCD curves at different current densities for PPy-100 (a-b), 150 (c-d), 200 (e-f), 250 (g-h), 300 (i-j) filter paper based symmetric aqueous supercapacitor, respectively.

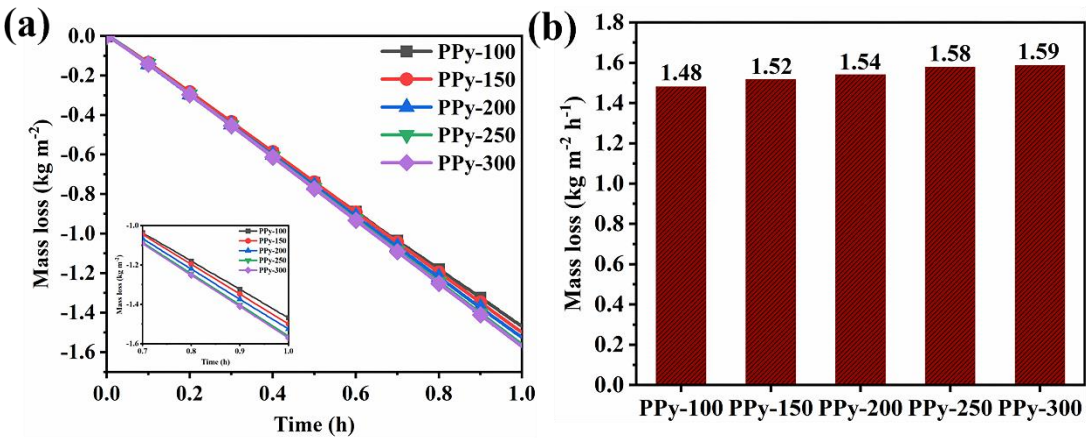

Figure S9. (a) The mass loss curve of pure water, (b) the solar evaporation rates of pure water for PPy-100, 150, 200, 250, 300 under 1 kW m^{-2}, inset: a local magnification image of the solar evaporation rates of pure water.

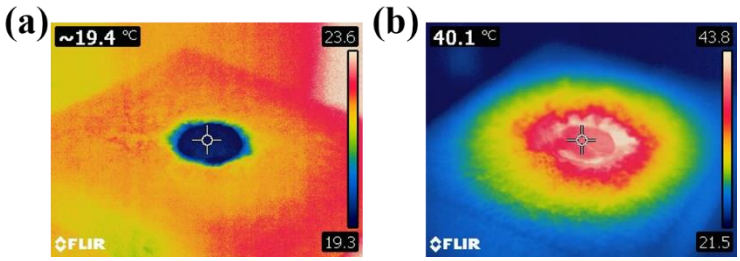

Figure S10. The IR images of the PP-PPy-200 under the illumination of 1 kW m^{-2} at (a) 0 min and (b) 60 min.

Heat conduction, radiation and convection are existing in the solar-driven water evaporation process.

(1) Heat conduction

The heat conduction could be calculated by the following formula:

$$q_{con} = \frac{cm\Delta T}{At} \quad \text{(S-1)}$$

In this formula:

q_{con} is the heat flux (W m^{-2});

c is the specific heat capacity (4.2× 10^3 J kg^{-1} k^{-1});

m is the bulk water mass (kg);

A is the heat conduction area (m^{-2});

t is the heat time (s);

ΔT is the temperature change of bulk water (K).

(2) Radiation

The radiation of solar-driven water evaporation could be calculated by the following formula:

$$q_{rad} = \varepsilon\sigma(T_2^4 - T_1^4) \quad \text{(S-2)}$$

In this formula:

q_{rad} is the radiation density (W m^{-2});

σ is the Stefan-Boltzmann constant (5.67× 10-8 W m^{-2} K^{-4});

ε is the emissivity of material; In this study, the emissivity of PP-PPy-200 is 0.593.

T_2 is the surface temperature of solar photothermal conversion material (K);

T_1 is the vapor temperature (K). In this study, the vapor temperature of PP-PPy-200 is 312.45 K.

(3) Convection

The convection of solar-driven water evaporation could be calculated by the following formula:

$$q_{conv} = h(T_2 - T_1) \quad \text{(S-3)}$$

In this formula:

q_{conv} is the convection density (W m^{-2});

h is the coefficient of convection (W m^{-2} K^{-1}). In this study, the coefficient of convection is 5 W m^{-2} K^{-1} according to previous studies.

T_2 is the surface temperature of solar photothermal conversion material (K);

T_1 is the vapor temperature (K).

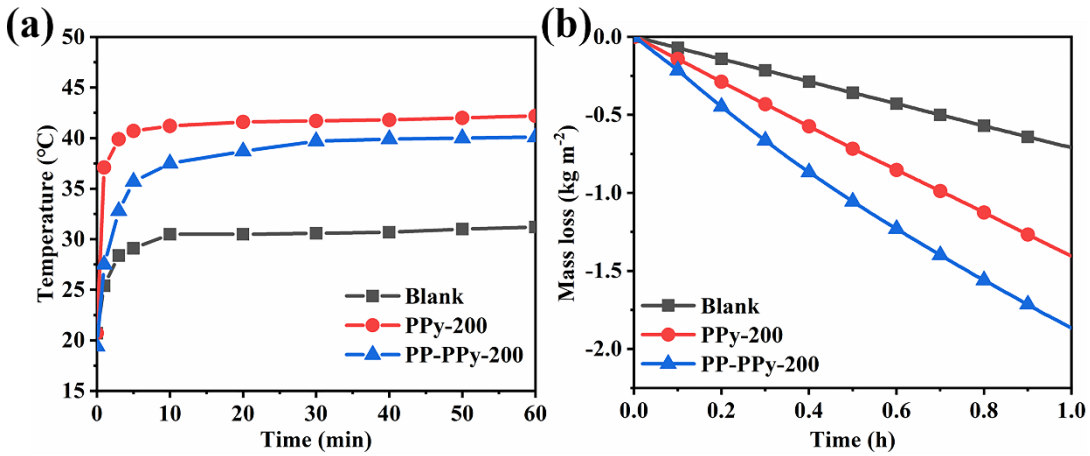

Figure S11. (a) Surface temperature of pure water, (b) the mass loss curve of pure water sea water in the East China Sea.

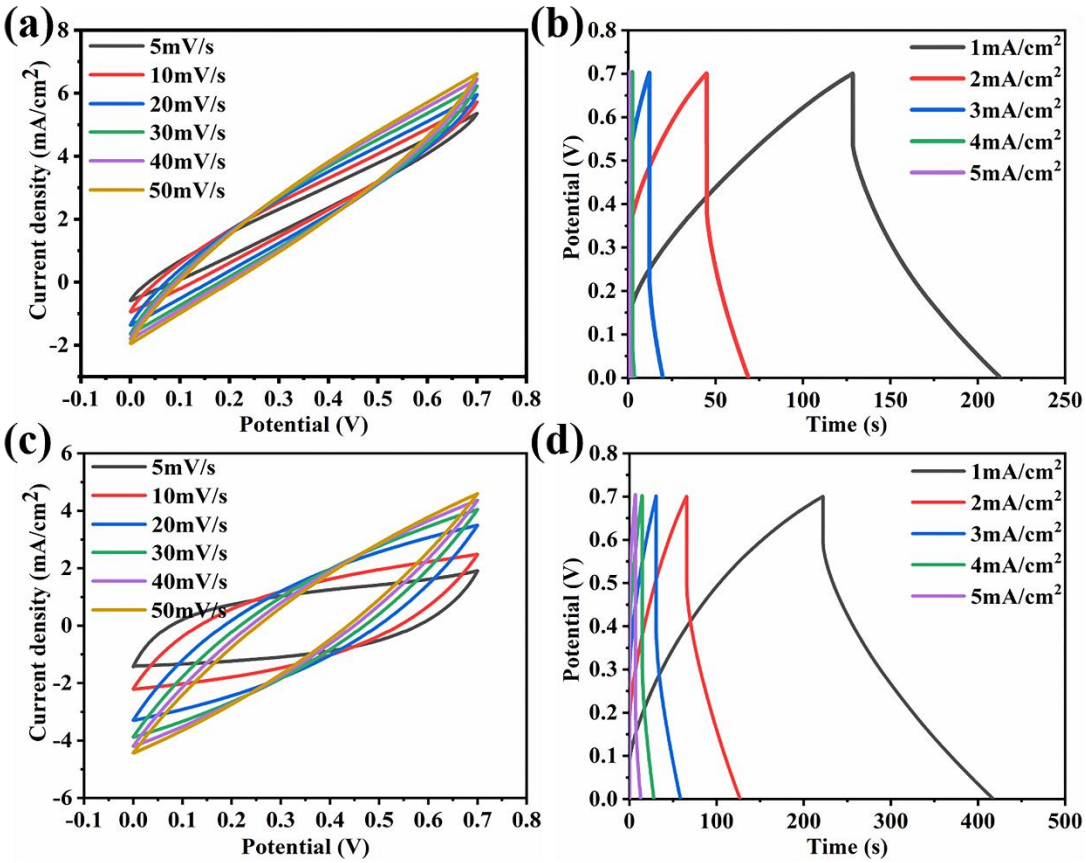

Figure S12. CV cures at different scan rates and GCD curves at different current densities for PP-PPy-200 (a-b) in the dark and (c-d) under one sun illumination, respectively.

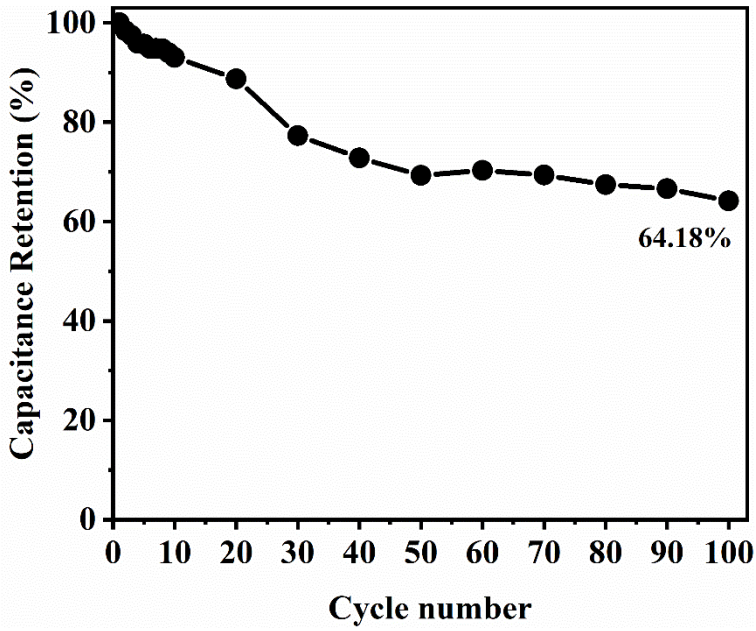

Figure S13. The cycling performance of PP-PPy-200 under one solar illumination.

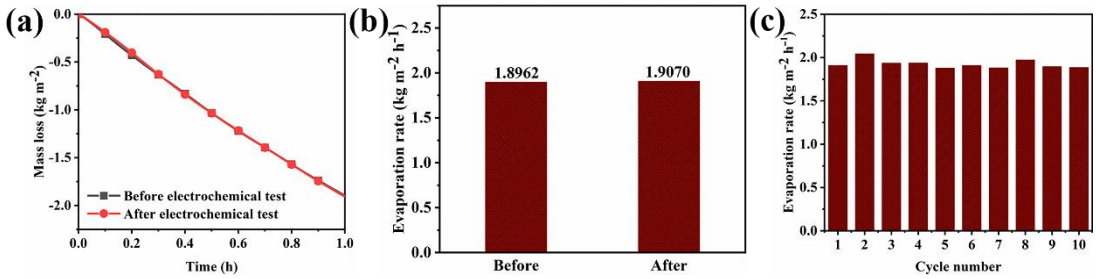

Figure 14. Solar-thermal evaporation performance of PP-PPy-200. (a) The mass loss curve before and after the GCD test, (b) the solar evaporation rates before and after the GCD test, (c) the cyclic evaporation performances of PP-PPy-200 under 1 kW m^{-2}.

References

1. L. N. Ma, R. Liu, H. J. Niu, M. Zhao and Y. D. Huang, *Compos. Sci. Technol.*, 2016, **137**, 87-93.
2. T. Yue, A. I. Douka, K. Qi, Y. B. Qiu, X. P. Guo and B. Y. Xia, *J. Mater. Chem. A*, 2021, **9**, 21799-21806.
3. X. H. Yan, J. Y. Miao, J. J. Wang, H. Jiang, M. Y. You, Y. H. Zhu and J. M. Pan, *Mater. Sci. Eng. B-Adv.*, 2021, **269**, 115166.
4. Y. X. Chen, K. F. Cai, C. C. Liu, H. J. Song and X. W. Yang, *Adv. Energy Mater.*, 2017, **7**, 1701247.
5. Z.-H. Chang, D.-Y. Feng, Z.-H. Huang and X.-X. Liu, *Chem. Eng. J.*, 2018, **337**, 552-559.
6. J. Ren, M. Shen, Z. Li, C. Yang, Y. Liang, H.-E. Wang, J. Li, N. Li and D. Qian, *J. Power Sources*, 2021, **501**, 230003.
7. Y. Tian, J. Liu, X. Song, L. Zhao, P. Zhang and L. Gao, *Compos. Sci. Technol.*, 2020, **197**, 108263.